Bioactivity response of $Ta_{1-x}O_x$ coatings deposited by reactive DC magnetron sputtering

CrossMark

C.F. Almeida Alves [a,*], A. Cavaleiro [b], S. Carvalho [a,b]

[a] GRF-CFUM, Physics Departament, University of Minho, Campus of Azurem, Guimaraes 4800-058, Portugal
[b] SEG-CEMUC, Mechanical Engineering Department, University of Coimbra, Coimbra 3030-788, Portugal

ARTICLE INFO

ABSTRACT

The use of dental implants is sometimes accompanied by failure due to periimplantitis disease and subsequently poor esthetics when soft–hard tissue margin recedes. As a consequence, further research is needed for developing new bioactive surfaces able to enhance the osseous growth. Tantalum (Ta) is a promising material for dental implants since, comparing with titanium (Ti), it is bioactive and has an interesting chemistry which promotes the osseointegration. Another promising approach for implantology is the development of implants with oxidized surfaces since bone progenitor cells interact with the oxide layer forming a diffusion zone due to its ability to bind with calcium which promotes a stronger bond.

In the present report Ta-based coatings were deposited by reactive DC magnetron sputtering onto Ti CP substrates in an Ar + O_2 atmosphere. In order to assess the osteoconductive response of the studied materials, contact angle and in vitro tests of the samples immersed in Simulated Body Fluid (SBF) were performed. Structural results showed that oxide phases where achieved with larger amounts of oxygen (70 at.% O). More compact and smooth coatings were deposited by increasing the oxygen content. The as-deposited Ta coating presented the most hydrophobic character (100°); with increasing oxygen amount contact angles progressively diminished, down to the lowest measured value, 63°. The higher wettability is also accompanied by an increase on the surface energy. Bioactivity tests demonstrated that highest O-content coating, in good agreement with wettability and surface energy values, showed an increased affinity for apatite adhesion, with higher Ca/P ratio formation, when compared to the bare Ti substrates.

1. Introduction

Several materials have been proposed for use as dental implants, namely, 316L stainless steel (SS 316L) [1], chromium–cobalt–molybdenum alloy (Cr–Co–Mo) [2], hydroxyapatite (HAp) [3], zirconia (ZrO_2) and/or alumina (Al_2O_3) [4] but only a few of them have been accepted such as commercially pure titanium grade 2 (CP Ti Gr2) [5,6] and titanium–6aluminum–4vanadium alloy (Ti6Al4V–Ti Gr5) [7–10]. Currently, most dental implants are manufactured on CP Ti Gr2 or Ti Gr5, with threaded geometries with internal connections for the abutments [11]. Nowadays, conventional implants can be manufactured with a porous microstructure propitiating a more efficient bone tissue ingrowth by the increase of the specific surface in contact with the surrounding media [5]. Nevertheless, commercial dental implants still present a number of limitations and their use is sometimes accompanied by failure [12,13]. The slow osseointegration of Ti dental implants leads to slow loading of the implant by the artificial crown, thus requiring a long non-operational time [12,14], which enhances the probability of microorganisms entrance on the oral environment close to the surgical site, specifically to the surface of the dental implant. The adhesion and possible microbial colonization can induce the appearance of infections with consequent post-surgical complications [15,16]. Infections are the main responsible for the short, medium and long-term failure of the dental implants. Failure due to periimplantis disease, which is the most common, is related with the late infection of the adjacent bone tissue that makes the bone recede and subsequently a decrease in the mechanical anchorage of the implant is observed. As a consequence, when the soft–hard tissue recedes, the "gray" Ti is exposed with a consequent poor esthetics [17,18]. These limitations are mainly associated with the poor bioactivity of Ti (ability to stimulate the formation of new apatite containing tissue) [19]. For achieving the integration of the implant with the surrounding bone tissue, further research is needed for developing new highly bioactive surfaces able to enhance and promote the osseous growth and bone matrix mineralization.

In the last years, there has been a great interest in the modification of surface characteristics of dental implants as a demand for bioactive surfaces that enhance the implant healing process [20]. In our days tantalum (Ta) is pointed as a promising material since, comparing to Ti, it is bioactive and has interesting chemistry valences which promote a

* Corresponding author at: Universidade do Minho, Escola de Ciências, Departamento de Física, Campus de Azurém, 4800-058 Guimarães, Portugal.
E-mail address: cristiana.alves@fisica.uminho.pt (C.F. Almeida Alves).
URL: http://smf-materials.weebly.com/ (C.F. Almeida Alves).

higher biomineralization kinetics enhancing the osseointegration [13, 21–25]. According to Balla et al. [26] a layer of hydroxyapatite was rapidly formed on a Ta surface immersed in simulated body fluid (SBF), revealing a strong chemical bond due to the high surface energy of Ta, compared to CP Ti. In addition, Frandsen et al. [27] found that Ta shows a better biological behavior compared to titanium dioxide (TiO_2) surfaces, when alkaline phosphatase activity tests were performed. In fact, Ta revealed a faster rate of matrix mineralization ($\approx 30\%$) due to its surface chemistry properties.

The major drawback of Ta is its high cost, which makes Ta dental implants less cost effective [28]. However, since the bioactivity is determined by surface properties [29], the surface modification of the implants with Ta coatings represents a challenging selection for the development of bioactive surfaces.

Another promising approach for implantology is the development of implants with oxidized surfaces [30,31]. In fact, bone progenitor cells interact with the oxide layer forming a diffusion zone due to its ability to bind with calcium which promotes a stronger bond [23,24,32], besides enhancing the corrosion resistance [25,33]. Then, the surface modification of Ti implants with tantalum oxide coatings can also play an important role in the interface between the bone and the implant.

The aim of this work is the development of bioactive surfaces for dental implants by chemically modifying their surface through the deposition of bioactive $Ta_{1-x}O_x$ coatings deposited by DC magnetron sputtering. The influence of the oxygen partial pressure on the structure, morphology and topography of Ta-based films was analyzed. The coating's bioactivity was evaluated by in vitro tests through the samples immersion in Simulated Body Fluid (SBF).

Taking into account the recent developments on the new generation of porous implants, it may be possible to extend this deposition technique to porous implants by the adjustment of some deposition parameters.

2. Materials and methods

2.1. Coating deposition

$Ta_{1-x}O_x$ coatings were deposited by reactive DC magnetron sputtering from a high-purity Ta target (99.6% Ta) (200×100 mm^2) onto polished SS 316L (20×20 mm^2), stainless M5 screws (commercial implants geometry), chemical etched CP Ti Gr2 (ASTM: F67) (20×20 mm^2), and single crystalline silicon (Si) (100) (10×10 mm^2). The 316L SS substrates were polished using emery paper from 600 to 2400 grit and then mirror polished with a diamond solution, attaining a final surface roughness Ra < 3 nm. The substrates were ultrasonically cleaned in distilled water, ethanol and acetone for 10 min for each solvent. The depositions were carried out with the substrates rotating at constant speed of 7 rpm, at 70 mm far from the target. The deposition temperature was kept constant at approximately 200 °C.

Previously to coating deposition, the substrates were sputter-etched for 15 min. in argon (Ar) atmosphere (1.2 Pa) at constant current density (J_{Ta}) of 0.5 mA/cm^2 applied to Ta target and by applying a current of 500 mA to the substrate holder. This procedure allows to eliminate remaining impurities present on the target and substrates surface, as

well as to remove surface oxides. In order to improve the adhesion of the coatings, a Ta interlayer was deposited in all coatings, with a thickness of approximately 200 nm. The interlayer was deposited by applying a current density of 10 mA/cm^2 in Ar atmosphere (0.6 Pa) at constant bias voltage of -75 V. The depositions were carried out in Ar + O$_2$ atmosphere, with a constant bias voltage of -75 V. The current density was changed from 10 to 5 mA/cm^2 to achieve the reactive deposition mode, as indicated in Table 1. Ar flow was kept constant at 0.6 Pa while the reactive gas flow, O$_2$, was adjusted (in a range of 0.6–0.8 Pa discharge pressure) as can be depicted in Table 1. The base pressure in the deposition chamber was always better than 6×10^{-4} Pa.

The deposition onto M5 screws, geometry used in commercial dental implants, revealed that the thickness and morphology of the coatings are homogenous over the threaded geometry, similar to the observed planar substrates. Thus, due to the high cost of dental implants and in order to facilitate the coating characterizations, generic test specimens were used in the following characterizations.

2.2. Coating characterization

Coating chemical composition was determined in a Cameca SX50 electron probe microanalysis (EPMA) equipment, operating at 10 kV and 40 nA. Scanning electron microscopy (SEM) was used to measure the film thickness and evaluate the coating morphology. SEM analysis was performed using a LEICA S360 operating at 10 kV in secondary electron mode. The structure and phase distribution of the films were determined by X-ray diffraction (XRD), in a Bruker D8 Discover, operating at 40 kV and 40 mA, with Cu radiation ($\lambda k_{\alpha 1} = 0.1540600$ nm and $\lambda k_{\alpha 2} = 0.1544339$ nm), equipped with collimator. The experiments were carried out in grazing angle geometry (1°). All the tests were performed with a step size of 0.025° and a time per step of 2 s, in 10–80° range. The morphology/topography of the coatings was evaluated by atomic force microscopy (AFM) using a NanoScopeIII model from Digital Instruments operating in tapping mode. AFM images were taken over scanning areas of 5×5 μm^2 and, for each film, three different areas were analyzed. EPMA, SEM and XRD analysis were performed in coatings deposited onto Si substrates since it allows an easier and more accurate characterization. In fact, its very low roughness surface improves the homogeneity of the sample to be tested improving the reproducibility of the measurements. We are aware that the final products will not have this final finishing surface, but for comparison and optimization purposes, it is important to keep this homogeneity, AFM measurements were performed in coatings deposited onto Si and SS 316L substrates.

The adhesion between $Ta_{1-x}O_x$ coating and the substrate, SS 316L, was assessed by scratch test experiments using a Mikron VCE 500 equipment. For all samples, two scratch tests were performed using a diamond Rockwell indenter. The load was increased linearly in the range of 2–90 N with a rate of 10 N/min and a sliding speed of 10 mm/min. The critical load values (L_{C_3}) were determined by optical microscope observation of the scratch tracks. The critical loads correspond to severe delamination when more than 50% of the substrate is exposed [34].

Table 1
Chemical composition, deposition parameters, deposition rate and critical load of the deposited samples.

Sample	Chemical formula	Chemical composition (at.%)		O$_2$ Flow (sccm)	Current density (mA/cm^2)	Deposition rate (μm/h)	Critical load (L$_{C_3}$)
		Ta	O				
Ta1	$Ta_{0.95}O_{0.05}$	95 ± 0.3	5 ± 0.3	0	10	2.3	>80 N
TO1	$Ta_{0.89}O_{0.11}$	89 ± 0.6	11 ± 0.6	2	10	2.1	
TO3	$Ta_{0.73}O_{0.27}$	73 ± 0.2	27 ± 0.2	6	10	2.3	
TO5	$Ta_{0.57}O_{0.43}$	57 ± 0.2	43 ± 0.2	10	10	2.8	
TO6	$Ta_{0.40}O_{0.70}$	30 ± 0.4	70 ± 0.4	13	5	1.9	

2.3. Wettability measurements

Wettability is an important surface property of biomaterials that can regulate the protein adsorption and, subsequently, the cell behavior [35]. This paper follows the Van Oss approach [36] to characterize the samples surface as a hydrophilic or hydrophobic. Van Oss considers that a surface with contact angle above 65° is hydrophobic, while for values lower than 65° the surface is considered hydrophilic. Moreover, the calculation of the free surface energy (ΔG_{mwm}) also allows to classify quantitatively the hydrophilic/hydrophobic character of a surface. The surface free energy is the necessary work to expand the drop of liquid on a unit of area. In this case, when the surface free energy is negative the interaction between the molecules of the liquid and the surface of the sample is attractive and, thus, the surface poorly interacts with water, making it hydrophobic. Conversely, when the free surface energy becomes positive (≥ 0), the interaction is repulsive and, consequently, the surface is hydrophilic due to the higher interaction between the sample surface and the water. Therefore, zero free surface energy is the border between hydrophilic and hydrophobic surfaces [36].

The wettability characteristics of the surfaces were assessed by measuring the static contact angle in a DataPhysics OCA-15 apparatus with 3 μl of ultra-pure water, α-bromonaphtalene and formamide at room temperature and were performed in coatings deposited onto SS 316L substrates. For each sample, a minimum of eight measurements were taken, after allowing the system (air/water/surface) to reach equilibrium, and aftermost the average value was calculated.

More important than the determination of the static contact angle values between a surface and a pure liquid, is the determination of the surface free energy. The calculation of the surface free energy was based on the Young's equation [36], which describes the thermodynamic equilibrium of free surface energies which coexist in the boundary of a liquid droplet in a solid surface. Contact angle measurements allowed the calculation of coating hydrophobicity parameters using the Van Oss approach [36].

2.4. Bioactivity experiments

Bioactivity was evaluated by soaking the coating in 25 ml of simulated body fluid (SBF) which has ions concentration nearly equal to those of human blood plasma at 36.5 °C. SBF was prepared by dissolving NaCl, NaHCO$_3$, KCl, K$_2$HPO$_4$.3H$_2$O, MgCl$_2$.6H$_2$O, CaCl$_2$, and Na$_2$SO$_4$ into Milli-Q water and buffered at pH 7.40 at 36.5 °C with 45 mM of (CH$_2$OH)$_3$CNH$_2$ and appropriate amount of HCl using the Kokubo and Takadama approach [37]. After soaked, the samples were removed from SBF after 24 h, 7 and 14 days (d), cleaned with Milli-Q water and dried in a desiccator. The bioactivity tests were performed in coatings deposited onto SS 316L substrates. For each sample, three measurements were performed to statistically validate the results. SEM and energy dispersive X-ray spectroscopy (EDS) (NanoSEM — FEI Nova 200 (SEM); EDAX — Pegasus X4M (EDS) operating at 5 and 10 keV in secondary electron mode and in EDS mode, respectively) were used to study and evaluate the presence of calcium phosphates and the evolution of Ca/P ratio on the surface of the soaked samples. XRD was performed in Bragg–Brentano geometry (step size of 0.02° and time per step of 1 s) to detect vestiges of crystalline calcium phosphates and their phase composition.

3. Results

3.1. Physical and chemical characterization

Coating deposition parameters, their chemical composition and thickness are summarized in Table 1. When the oxygen (O) flow was increased from 0 sccm up to 10 sccm an increase in the oxygen content from 5 to 43 at.% was observed. The oxygen in the Ta coating could be attributed to residual O$_2$ present in the deposition chamber. Concerning

the deposition rate, no significant changes were observed with increasing O$_2$ flow up to 10 sccm. As target potential values also do not change significantly (from 349 to 416 V), the depositions are still being performed in metallic mode. In order to further increase the oxygen amount in the coating, the J$_{Ta}$ was reduced from 10 mA/cm^2 to 5 mA/cm^2 and the O$_2$ flow was set to 13 sccm. The increase in target potential value (537 V), in spite of the much lower target current used in the deposition, suggests that the coating was now deposited in compound mode, reaching an oxygen content of 70 at.%.

For application in biomedical devices, coating adhesion onto the implant is an important characteristic to be considered. Scratch testing results revealed a remarkable adhesion behavior for all coatings taking into account that a soft steel substrate is being used (SS 316L). In fact, the critical load values are higher than 80 N in all tested samples.

3.2. Structural analysis

XRD analyses were carried out in order to understand the evolution of the structure with the increase of the oxygen content. The XRD patterns are shown in Fig. 1 and the main identified crystalline phases are α-Ta: body-centered cubic (bcc) (ICDD card n° 00-004-0788) and β-Ta: tetragonal (ICDD card n° 00-025-1280). The differences in the chemical composition correlated well with the differences observed in the developed structure.

Ta1 coating crystallized in a bcc which represents the typical structure of α-Ta. When oxygen was added to Ta, a change in the bcc structure to a mixture of α-Ta (bcc) and β-Ta (tetragonal) was achieved. With further addiction of oxygen, XRD peaks enlarges and becomes less defined suggesting that Ta phases became nanocrystalline. Still, oxides phases such as bcc Ta$_2$O (ICDD 01-074-2305), tetragonal TaO$_2$ (ICDD card n° 00-019-1297) and/or Ta$_2$O$_5$ (Orthorhombic ICDD card n° 01-070-9177 or Base centered monoclinic ICDD card n° 01-070-4776) cannot be disregarded since they also have diffraction lines centered in the main broad peak (see Fig. 1b). The coating with 70 at.% of oxygen deposited in reactive compound mode revealed an amorphous structure, as suggested by the absence of diffraction peaks in the XRD pattern.

3.3. Morphology and topography assessment

The morphology and topography of each coating was analyzed by SEM and AFM, respectively, and the results are depicted in Fig. 2. In general the films revealed fairly uniform deposition. The AFM results are very well correlated with the surface morphology disclosed by SEM images. The AFM and SEM micrographs of Ta1 and TO1 coatings are characterized by cauliflower-like patterns, which generally are observed in coatings grown with typical columnar morphologies. The coatings with higher amounts of oxygen showed a smooth surface which is typical of very compact coatings with featureless morphology.

The roughness values obtained from AFM analysis of coatings deposited on Si substrates are shown in Table 2. The increase of oxygen content on the coatings promotes a significant decrease of the mean roughness values. Ta1 and TO1 coatings showed similar topographies/morphologies with very similar roughness values (see Table 2), while the coatings with higher oxygen contents showed smoother surfaces with lower roughness. The slight increase in roughness values of the coating deposited in compound mode might be related with the different deposition parameters: decrease in J$_{Ta}$ and increase in O$_2$ flow (see Table 1).

The roughness values of CT Ti Gr2 (used in commercial dental implants) and SS 316L bulk materials as well as Ta$_{1-x}$O$_x$ coatings deposited on SS 316L substrates are shown in Table 3. The roughness of the coatings deposited onto SS 316L follows the same trend as the coatings deposited on Si substrates (see Table 2), with slightly higher values, attributed to the higher roughness of the substrate.
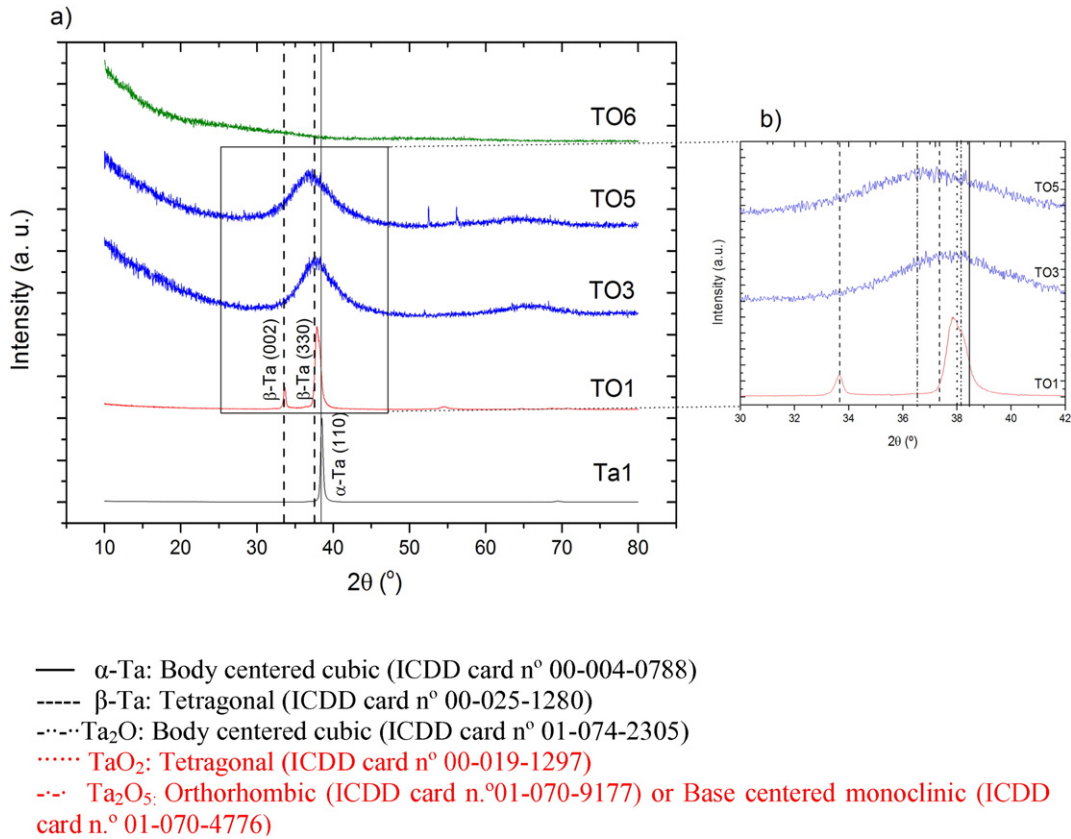
Fig. 1. Grazing incidence XRD patterns of the coatings as a function of the oxygen content, deposited onto Si substrates.

3.4. Wettability analysis

The measured contact angle values and the surface free energy of the samples are presented in Table 4. CP Ti Gr2 was used as the commercial surface control.

In view of Milli-Q water, Ta1 surface has a much higher contact angle (around 100°) than the control CP Ti Gr2 (approximately 74°) being assumed as the sample with the most hydrophobic character. With the increase of oxygen content in the coatings a decrease of the contact angle values was observed with values from 81° down to 63°.

Regarding the surface free energy values, similar trends were observed, Ta1 coating showed the lowest free surface energy (-97 mJ/m^2), less than the CP Ti Gr2 control. Oxygen-containing coatings have increasing free surface energies, in the range from -65 mJ/m^2 up to -31 mJ/m^2, with increasing oxygen contents. All analyzed samples showed a typical hydrophobic behavior (with a surface energy value below zero). TO6 surface has the highest value of surface free energy, thus, indicating a lower degree of hydrophobicity, which is in accordance with its contact angle value slightly below 65° (63°). These results suggest that TO6 sample has some polar interaction with the liquids.

3.5. Bioactivity response

In order to analyze the osteoconductive response of the studied materials and their potential for use in bone tissue replacement of dental implants, bioactivity tests were performed in SBF. The bioactive character allows to analyze the ability for apatite formation at the material surface after immersion in SBF, which intends to simulate the human blood. The bioactivity tests were performed in three samples, CP Ti Gr2, Ta1 and TO6; the first serving as standard and the two coatings

which presented the threshold values measured for the contact angle and the surface free energy.

Fig. 3 shows SEM micrographs of the surfaces of the three studied samples before and after immersion in SBF for 14 days. Note that the results for samples before soaking in SBF are, hereafter, denoted as 0 h. The SEM micrographs show the different morphology of the calcium phosphate formed on the surfaces after 14 days of immersion in SBF.

The presence of Ca and P was verified by EDS technique, the mean ratio Ca/P was determined by the average of three EDS measurements in different zones of the sample. It should be pointed out that before 7 days, no calcium phosphates was detected in any of the analyzed surfaces. After 7 days only for the CP Ti Gr2 sample signs of calcium phosphates were not observed. After 14 days of exposure the Ca/P atomic ratio on the surface of the coating with 70 at.% oxygen, TO6, was 1.73 approaching the ratio of natural hydroxyapatite (1.67 according to the literature [38]). Calcium phosphates were also observed on the Ta1 surface, with a ratio Ca/P close to the natural hydroxyapatite (1.57). The CP Ti Gr2 control showed the worst bioactive behavior since, by EDS, the calcium phosphates visible in the surface show a Ca/P ratio very far from the natural hydroxyapatite, specifically 0.95.

Fig. 4 shows the XRD results of the immersed samples in SBF after 14 days. Ta1 and TO6 samples showed the presence of a crystalline phase based on calcium phosphates as suggested by EDS results. This apatite is strongly oriented, not being detected any other XRD peak in the diffractogram, which does not allow to precisely identify which apatite structure in being formed. The crystallinity degree is significantly higher in Ta1 than for TO6 surface. On the other hand, CP Ti Gr2 only showed peaks corresponding to the hexagonal Ti phase (ICDD card n° 00-044-1294) suggesting that the formed calcium phosphates in its surface is in very low amount.
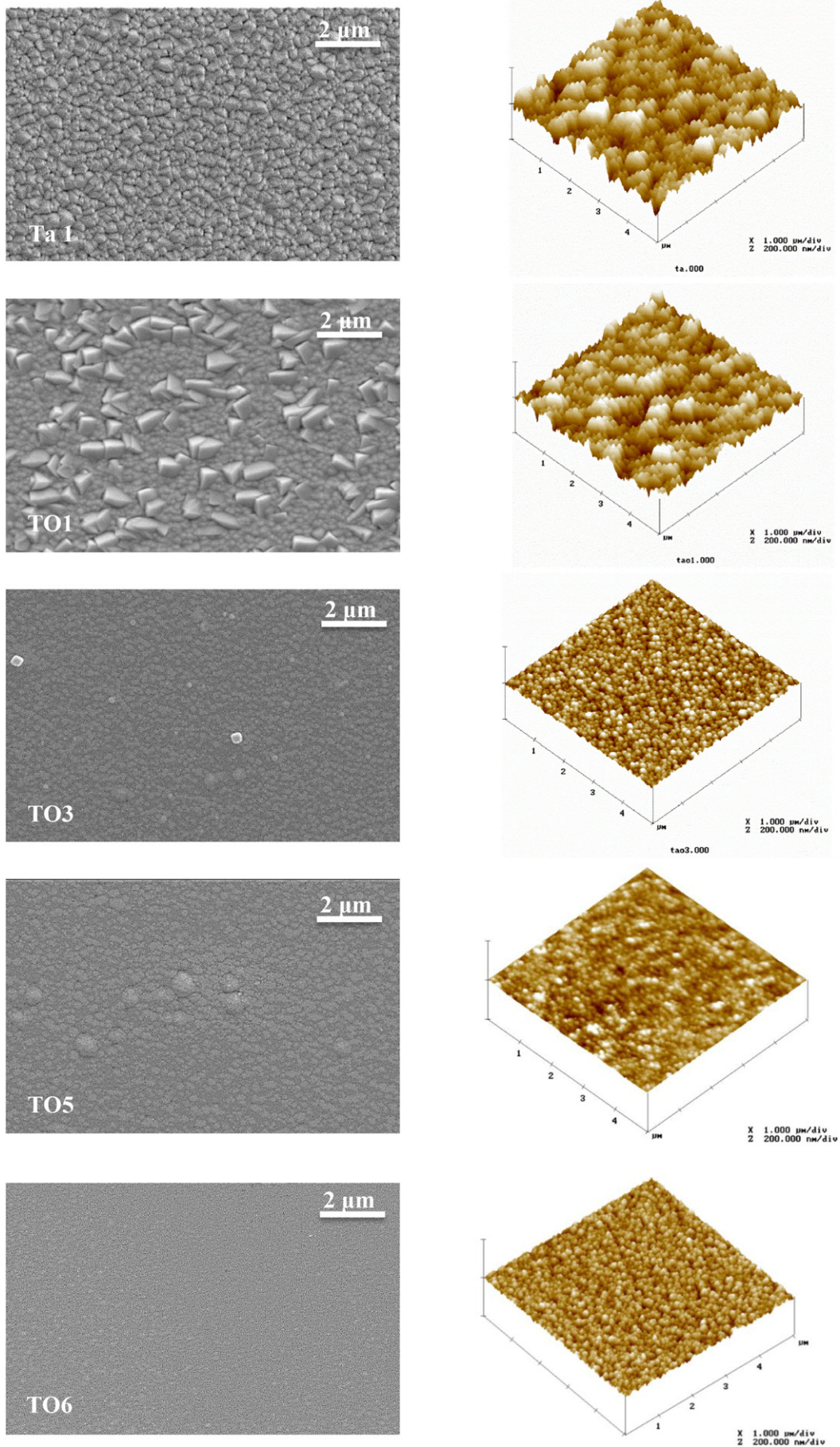
Fig. 2. SEM and AFM micrographs of $Ta_{1-x}O_x$ coatings as a function of the oxygen content, deposited onto Si substrates.

Table 2
Ra, Rq and Rmax values of the coatings, deposited on Si, as a function of oxygen content, measured by AFM and resulting from an average of three different zones.

Sample	Ta1	TO1	TO3	TO5	TO6
Ra (nm)	17 ± 1.0	17 ± 0.32	3.4 ± 0.098	1.3 ± 0.12	4.3 ± 0.039
Rq (nm)	21 ± 1.4	21 ± 0.49	4.2 ± 0.13	1.8 ± 0.16	5.4 ± 0.050
Rmax (nm)	172 ± 17	169 ± 7.1	34 ± 3.6	15 ± 2.9	47 ± 0.67

4. Discussion

4.1. Coating production

The elemental chemical composition showed, as it would be expected, that by increasing the O_2 flow, the oxygen content increases from 5 up to a maximum value of 70 at.%. The oxygen in Ta1 film is attributed to residual O_2 in the deposition chamber. Concerning the deposition rate, up to O_2 flows of 10 sccm, the incorporation of oxygen in the growing film leads to higher values. However, when the current density changes to 5 mA/cm^2 and the O_2 flow was set to 13 sccm, the deposition rate decreased dramatically, due to the marked reduction of the sputtering yield of the target either related to the reduction of current density (half of value) or to the poisoning effect of the target. This behavior is similar to that achieved by Chandra et al. [39] in the deposition of tantalum oxides coatings, Cristea et al. [40] in TaON films or Vaz et al. [41] in ZrON coatings, in all cases deposited by reactive sputtering.

XRD revealed the body-centered cubic phase, α-Ta, for Ta1 coating. According to Chandrasekhar et al. [42] the occurrence of this phase at relatively low deposition temperatures, compared to the results of other authors [28], is explained by the application of negative bias during the deposition. When the oxygen content increased to 11 at.% the crystal structure changed to a mixture of α-Ta and β-Ta phases. This behavior was also observed by Zhou et al. [43,44] in the Ta–O system for reactive sputtering with low O_2/Ar flow ratio. According to Kepner et al. [45] the incorporation of oxygen in the coating leads to a distortion in the structure of α-Ta phase (stable phase), due to its low solubility in this phase (≤ 1.4 at.%), promoting the formation of β-Ta phase [45]. For films with intermediate oxygen content (TO3 and TO5) the broad diffraction band at 37° suggests that the coating is nanocrystalline making difficult an unequivocal identification of the phase or phases occurring. In fact, in this zone, diffraction peaks of tantalum and sub-stoichiometric tantalum oxide phases, such as α-Ta, β-Ta, Ta_2O, TaO_2 and/or Ta_2O_5 phases may occur. Yang et al. [31] also reported this band on tantalum oxide coatings deposited by reactive sputtering. With increasing oxygen content, there is a shift of the band to the left that can be associated with the increase of the inter-atomic distance induced by the presence of further oxygen species.

The coating with the highest oxygen content was amorphous. This behavior is usually observed for other oxygen-containing compounds deposited by reactive magnetron sputtering as, for example, W–O [46], W–O–N [47], TiC_xO_y [48] and Ti–Si–C–N–O [49]. According to the literature [50], the incorporation of oxygen in the crystal lattice causes the deformation of the initial metal structure promoting initially the precipitation of oxides in the grain boundaries, inhibiting the grain growth and decreasing the grain size, and leading, in a second step, to the formation of amorphous structure [50].

The cauliflower-like patterns developed by Ta1 and TO1 coatings are characteristic of coatings grown with low adatom mobility and

Table 4
Milli-Q water (θ_w), formamide (θ_F) and α-bromonaphtalene ($\theta_{\alpha-B}$) contact angles, surface energy components (apolar Lifshitz–Van der Waals surface free energy component, γ^{LW}; electron acceptor surface free energy component, γ^+; and electron donor surface free energy component, γ^-) and surface free energy of the coatings as a function of oxygen content, deposited onto SS 316L substrates.

Sample	Contact angle $\pm$ SD[a] (deg)			Surface energy components (mJ/m^2)			ΔG_{mwm} (mJ/m^2)
	θ_w	θ_F	$\theta_{\alpha-B}$	γ^{LW}	γ^+	γ^-	
CP Ti Gr2	74 ± 2.8	48 ± 3.1	25 ± 1.4	40	0.46	7.3	-46
Ta1	100 ± 4.8	67 ± 3.9	36 ± 1.5	36	0.20	0	-97
TO1	81 ± 2.9	47 ± 3.1	23 ± 4.1	41	0.97	2.1	-65
TO3	70 ± 1.7	50 ± 2.0	28 ± 1.7	39	0.23	12	-35
TO5	71 ± 2.8	49 ± 1.9	24 ± 0.75	41	0.28	10	-40
TO6	63 ± 2.8	38 ± 3.5	21 ± 0.98	41	0.89	13	-31

[a] Standard deviation.

relatively high discharge pressures, with typical columnar morphologies [51]. TO1 film shows sharp edges particles over the coating surface. This morphology, according with Zhou et al. [43], is related with the mixture of α and β Ta phases, which is in good agreement with XRD results. The surface micrographs (see Fig. 2) show that the increase in oxygen content promoted the coating densification, showing the smooth surface typical of very compact and cross section featureless coatings. These results are confirmed by AFM analysis, which showed decreasing Ra and Rq roughness values with increasing oxygen content. Banakh et al. [52] observed the same trend in TaON coatings deposited by reactive sputtering. In other similar systems as W–O [53] and W–O–N [47] this behavior was also found.

4.2. In vitro behavior

Surface wettability is an important parameter which should be taken into account for tissue engineering applications [54]. This physicochemical property does not affect directly the cell response, but can regulate the adsorption of the most important proteins from the culture medium, such as fibronectin and vitronectin, which will mediate the cell response and improve the cell adhesion [55]. As reported, moderately hydrophilic ($\approx 70–60°$) surfaces tends to adsorb the adhesion-promoting proteins (fibronectin and vitronectin) which will improve the cell attachment [56].

The contact angle tests showed that Ta1 surface has the highest value, around 100°, then presenting the most hydrophobic character ($\theta > 65°$). The increase of oxygen content on the coatings caused a decrease of the contact angle, due to the growing oxidation of the films, as it was shown by Sharma and Paul [57].

From literature [27], based on the surface chemistry, for Ta1 sample a lower contact angle in relation to control surface, CP Ti Gr2, was expected (31° and 54° respectively). Such trend was not observed in this study. This discordant result can be explained by the significant difference in the roughness values of the tested samples. In fact, the commercial control sample has a much higher Ra value than Ta sample, factor which is known to have a great influence on the contact angle [58–60].

According to the literature [36], for $Ta_{1-x}O_x$ coatings, at the observed levels of roughness the influence on the wettability is not clear. Therefore, these results suggest that the surface chemistry (increase of the oxygen content) is predominant on the regulation of the wettability.

Table 3
Ra, Rq and Rmax values of CP Ti Gr2 and SS 316L bulk materials as well as $Ta_{1-x}O_x$ coatings deposited on SS 316L, measured by AFM and resulting from an average of three different zones.

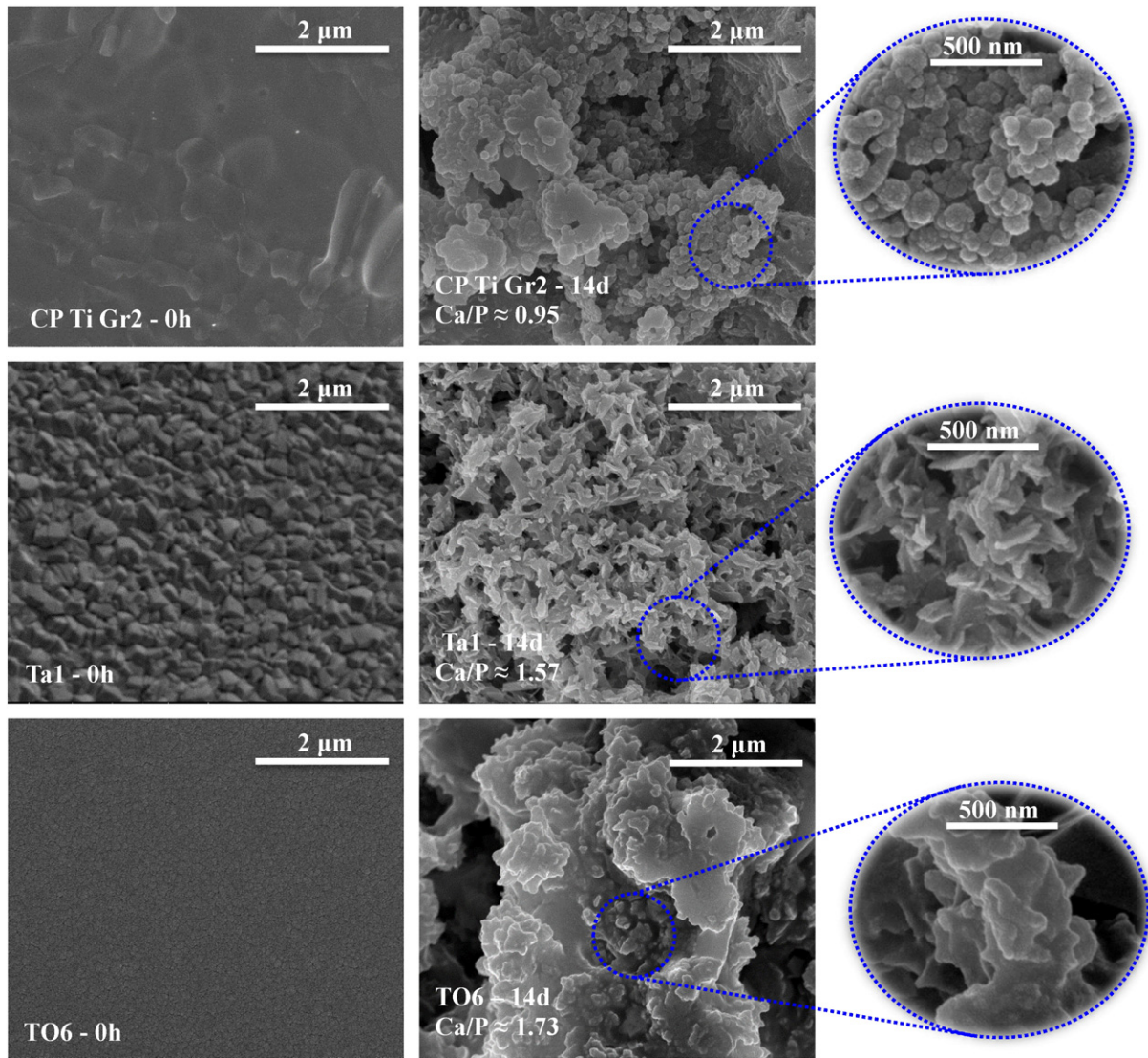| Sample	CP Ti Gr2	SS 316L	Ta1	TO1	TO3	TO5	TO6
Ra (nm)	71 ± 39	2.5 ± 0.11	21 ± 2.2	21 ± 1.8	7.8 ± 0.61	5.1 ± 0.57	5.8 ± 0.40
Rq (nm)	88 ± 49	3.4 ± 0.25	26 ± 2.6	31 ± 2.6	9.9 ± 0.77	6.4 ± 0.69	8.2 ± 0.53
Rmax (nm)	503 ± 250	44 ± 3.1	201 ± 6.3	305 ± 42	109 ± 28	54 ± 5.9	103 ± 17

Fig. 3. SEM micrographs of studied samples, CP Ti Gr2, Ta1 and TO6, respectively, before and after 14 days of immersion in SBF at 37 °C.

Both polar surface energy components ($\gamma+$ and $\gamma-$) of Ta1 and TO1 samples are close to zero which indicates that the surface is predominantly apolar. However, with the increase of oxygen content, the negative polar surface energy component ($\gamma-$) starts to increase significantly, indicating that the surfaces become monopolar. All samples showed qualitatively a hydrophobic behavior in agreement with their low surface energy, excepting the coating with the highest oxygen content (TO6) which showed a contact angle value slightly below of 65° (63°). This value is indicative of polar surface interaction typical to moderately hydrophilic surfaces. A better cell adhesion to hard tissue (bone) is expected for this sample since, for moderately hydrophilic and negatively charged surfaces the adsorption of cells is enhanced [54,61,62]. Bacakova et al. [61], showed that a contact angle close to 63° is an optimum value for osseointegration.

$Ta_{1-x}O_x$ samples showed better ability to change and adsorb ions of SBF and, consequently, better bioactivity performance comparatively to the group control CP Ti. After 14 days of immersion in SBF, both Ta-based surfaces showed Ca/P values close to that of hydroxyapatite ($Ca/P \approx 1.67$), particularly the oxide coating with a value of 1.73. The commercial surface control of CP Ti Gr2 shows the lowest Ca/P ratio suggesting that the osseointegration process should be slower. This fact proves that the bioactivity kinetics of $Ta_{1-x}O_x$ surfaces is faster than that of Ti surface favoring a faster osseointegration.

In the oxide sample the adhesion of ions of the fluid, namely Ca^{2+}, to the surface of the sample was significantly superior, what was expected since this sample showed a surface free energy close to zero and a lower contact angle around 63°, reported as optimum conditions for osseointegration. According to Kokubo et al. [63,64], oxide surfaces are the best option for the interaction with the fluid. From literature [24], when a Ta oxide (such as TO6) surface is soaked in SBF, by ion exchange, hydration of Ta–O occurs and Ta–OH groups are formed, providing favorable sites for the calcium phosphates nucleation. The Ta–OH groups bind to Ca^{2+} ions forming a calcium tantalate which, then, binds to PO_4^{3-} ions to form apatite. The bone progenitor cells interact with the oxide phase through this diffusion layer; the chemical bonding established between the functional groups (Ta–OH) and the calcium phosphate ions promotes a stronger bond between the dental implant surface and the cells. As verified, the Ta–OH groups induce a faster apatite nucleation by increasing the ionic activity at the surface. Therefore the oxidation state of the surface is benefic for the exponentiation of osseointegration [24].

Ta1 sample also demonstrated a high ability to bind with calcium phosphate ions even though only a residual content of oxygen exists. The high passivation rate of Ta and the oxide layer formed on the top [57] have a fundamental role for the formation of Ta–OH groups when the sample is soaked in SBF. For the control surface, CP Ti Gr2, although
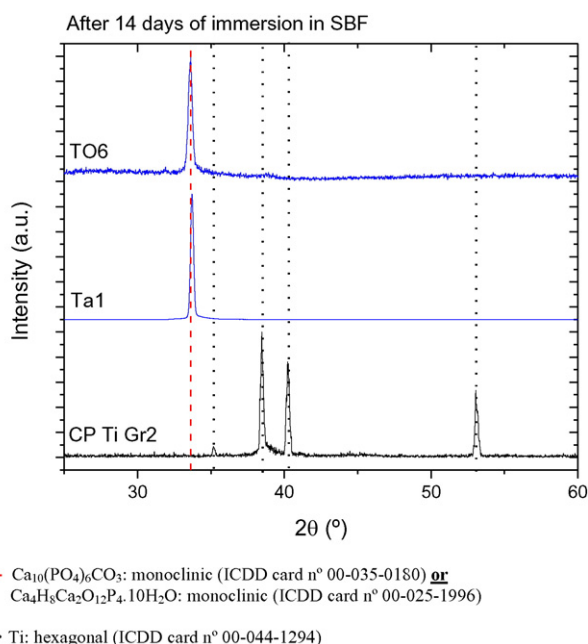
Fig. 4. XRD patterns of CP Ti Gr2, Ta1 and TO6 surfaces, respectively, after 14 days of immersion in SBF at 37 °C.

Ti also has a high passivation rate [65], it does not so easily promote apatite formation. The surface chemistry of Ta-based and Ti-based surfaces is different which, as reported by Frandsen et al. [27], causes a significant difference in the adhesion of the calcium phosphate ions.

Concerning the Ca/P atomic ratio estimated by EDS, it is possible to observe that there is a difference between the values of Ta1 sample and TO6 sample. These differences can be explained by the presence of carbon in the calcium phosphates, as detected by EDS measurements. As it is known, apatite is a flexible mineral that needs several elements to grow, such as, Ca, P, O and the appropriated channel-filling ions (OH^-, Cl^-, F^-, CO_3^{2-}) [66]. Subsequently, these ions allow several chemical substitutions determining the apatite structure. Usually the bone is an OH^- containing apatite with a very specific structure and composition [38]. According to the literature [67], the biomimetic way to induce the apatite growth as proposed by Kokubo and Takadama [37], also used in this study, leads to a carbonate containing bone-like apatite [67]. The carbonate substitution in the apatite structure can occur through 2 different ways: in the OH-site as "A-type" substitution; or in the PO_4-site as "B-type" substitution. Hence, it is suggested that in the present study the differences of the Ca/P atomic ratio values are related to the type of C substitution, in Ta1 surface should be of A-type whereas for TO6 of B-type [38].

After 14 days of immersion, the changes in the morphology of the calcium phosphates of the soaked samples is mainly dictated by the Ca/P ratio. The morphology of the calcium phosphate in the control surface is a typical cauliflower-like apatite cluster [68] whereas, in the $Ta_{1-x}O_x$ surfaces the morphology of the calcium phosphates evolve to a needle shaped-like layered apatite [69,70]. These needles are composed by a lot of densely packed lamellas of crystalline apatite [67]. This morphology is very promising since it is similar to that of the apatite which constitutes the bone [70].

The XRD results (see Fig. 4) are not conclusive since only one peak, around 33.86°, is detected in the pattern. However, considering the chemical composition estimated by EDS, showing the presence of carbon on the calcium phosphates, this peak can be assigned to either a monoclinic calcium phosphate carbonate (ICDD card n° 00-035-0180) or a monoclinic calcium tetraphosphonate decahydrate (ICDD card n° 00-025-1996). The lower crystallinity degree of TO6 sample can be related with the above type of carbonate substitution in the apatite

structure. In fact, in the B-type substitution suggested for the Ta oxide sample, the amorphous carbonate is incorporated into the apatite structure in the PO_4-site, which can leads to a decrease of the apatite crystallinity. The XRD pattern of the commercial control surface, CP Ti Gr2, only shows peaks corresponding to the hexagonal Ti phase which suggest that the presence of calcium phosphates in the surface is very low and, therefore, undetectable by XRD.

5. Conclusion

$Ta_{1-x}O_x$ coatings with different oxygen content were successfully deposited by reactive magnetron sputtering. Structural analysis revealed that the coatings with low and intermediate oxygen content showed a mixture of Ta and Ta (sub)oxide phases with a nanocrystalline structure; while the coating with the highest oxygen content proved to be amorphous. The increase in the oxygen amount retrieved more compact and smother $Ta_{1-x}O_x$ coatings. Contact angle measurements revealed that Ta1 coating presented the most hydrophobic character (100°). Besides, the increase of oxygen content caused the decrease on the contact angle values with TO6 coating depicting the lowest value, about 63°. Bioactivity tests showed the presence of calcium phosphates after 7 days of immersion in SBF, only for $Ta_{1-x}O_x$ samples. This behavior was confirmed after 14 days of exposure since Ca/P ratio values of 1.57 and 1.73 were measured for Ta1 coating and TO6 coatings, respectively, close to the hydroxyapatite value (Ca/P $\approx$ 1.67). The commercial surface control CP Ti Gr2 showed a much lower Ca/P ratio of 0.95, meaning that the osseointegration was not well enhanced as for the promising $Ta_{1-x}O_x$ whereas surfaces.

References

[1] J. Disegi, L. Eschbach, Stainless steel in bone surgery, Injury 31 (2000) D2–D6.
[2] M. Plecko, C. Sievert, D. Andermatt, R. Frigg, P. Kronen, K. Klein, S. Stübinger, K. Nuss, A. Bürki, S. Ferguson, Osseointegration and biocompatibility of different metal implants — a comparative experimental investigation in sheep, BMC Musculoskelet. Disord. 13 (2012) 1471–1483.
[3] J.L. Ong, D.C. Chan, Hydroxyapatite and their use as coatings in dental implants: a review, Crit. Rev. Biomed. Eng. 28 (2000) 667–707.
[4] B. Reinhardt, T. Beikler, Chapter 4 — dental implants, in: J.Z. Shen, T. Kosmač (Eds.), Advanced Ceramics for Dentistry, Butterworth-Heinemann, Oxford 2014, pp. 51–75.
[5] M. Oliveira, L. Pereira, C. Cairo, Porous structure characterization in titanium coating for surgical implants, Mater. Res. 5 (2002) 269–313.
[6] O.E. Pohler, Unalloyed titanium for implants in bone surgery, Injury 31 (2000) D7–D13.
[7] H. Rack, J. Qazi, Titanium alloys for biomedical applications, Mater. Sci. Eng. C 26 (2006) 1269–1277.
[8] J. Disegi, Titanium alloys for fracture fixation implants, Injury 31 (2000) D14–D17.
[9] X. Ye, L. Wang, Z.T.H. Tse, G. Tang, G. Song, Effects of high-energy electro-pulsing treatment on microstructure, mechanical properties and corrosion behavior of Ti–6Al–4 V alloy, Mater. Sci. Eng. C 49 (2015) 851–860.
[10] X. Ye, Y. Yang, G. Tang, Microhardness and corrosion behavior of surface gradient oxide coating on the titanium alloy strips under high energy electro-pulsing treatment, Surf. Coat. Technol. 258 (2014) 467–484.
[11] L. Vidyasagar, P. Apse, Dental implant design and biological effects on bone–implant interface, Balt. Dent. Maxillofac. J. 6 (2004) 51–54.
[12] A. Maho, S. Linden, C. Arnould, S. Detriche, J. Delhalle, Z. Mekhalif, Tantalum oxide/carbon nanotubes composite coatings on titanium, and their

functionalization with organophosphonic molecular films: a high quality scaffold for hydroxyapatite growth, J. Colloid Interface Sci. 371 (2012) 150–158.

[13] M. Roy, V.K. Balla, A. Bandyopadhyay, S. Bose, MgO-doped tantalum coating on Ti: microstructural study and biocompatibility evaluation, ACS Appl. Mater. Interfaces 4 (2012) 577–580.

[14] S.E. Kim, J.H. Lim, S.C. Lee, S.-C. Nam, H.-G. Kang, J. Choi, Anodically nanostructured titanium oxides for implant applications, Electrochim. Acta 53 (2008) 4846–4851.

[15] Z.H. Baqain, W.Y. Moqbel, F.A. Sawair, Early dental implant failure: risk factors, Br. J. Oral Maxillofac. Surg. 50 (2012) 239–243.

[16] L. Zhang, C. Ning, T. Zhou, X. Liu, K.W. Yeung, T. Zhang, Z. Xu, X. Wang, S. Wu, P.K. Chu, Polymeric nanoarchitectures on Ti-based implants for antibacterial applications, ACS Appl. Mater. Interfaces 6 (2014) 17323–17345.

[17] M. Esposito, J. Hirsch, U. Lekholm, P. Thomsen, Biological factors contributing to failures of osseointegrated oral implants. (I) Success criteria and epidemiology, Eur. J. Oral Sci. 106 (1998) 527–551.

[18] R. Dimitriou, G. Babis, Biomaterial osseointegration enhancement with biophysical stimulation, J. Musculoskelet. Nueronal Interact. 7 (2007) 253–265.

[19] M.G. Gandolfi, P. Taddei, F. Siboni, E. Modena, E.D. De Stefano, C. Prati, Biomimetic remineralization of human dentin using promising innovative calcium-silicate hybrid "smart" materials, Dent. Mater. 27 (2011) 1055–1069.

[20] A. Mavrogenis, R. Dimitriou, J. Parvizi, G. Babis, Biology of implant osseointegration, J. Musculoskelet. Nueronal Interact. 9 (2009) 61–71.

[21] V.K. Balla, S. Banerjee, S. Bose, A. Bandyopadhyay, Direct laser processing of a tantalum coating on titanium for bone replacement structures, Acta Biomater. 6 (2010) 2329–2334.

[22] Y. Leng, H. Sun, P. Yang, J. Chen, J. Wang, G. Wan, N. Huang, X. Tian, L. Wang, P. Chu, Biomedical properties of tantalum nitride films synthesized by reactive magnetron sputtering, Thin Solid Films 398 (2001) 471–475.

[23] B.R. Levine, S. Sporer, R.A. Poggie, C.J. Della Valle, J.J. Jacobs, Experimental and clinical performance of porous tantalum in orthopedic surgery, Biomaterials 27 (2006) 4671–4681.

[24] T. Miyazaki, H.-M. Kim, T. Kokubo, C. Ohtsuki, H. Kato, T. Nakamura, Mechanism of bonelike apatite formation on bioactive tantalum metal in a simulated body fluid, Biomaterials 23 (2002) 827–832.

[25] N. Wang, H. Li, J. Wang, S. Chen, Y. Ma, Z. Zhang, Study on the anticorrosion, biocompatibility, and osteoinductivity of tantalum decorated with tantalum oxide nanotube array films, ACS Appl. Mater. Interfaces 4 (2012) 4516–4523.

[26] V.K. Balla, S. Bodhak, S. Bose, A. Bandyopadhyay, Porous tantalum structures for bone implants: fabrication, mechanical and in vitro biological properties, Acta Biomater. 6 (2010) 3349–3359.

[27] C.J. Frandsen, K.S. Brammer, K. Noh, G. Johnston, S. Jin, Tantalum coating on TiO₂ nanotubes induces superior rate of matrix mineralization and osteofunctionality in human osteoblasts, Mater. Sci. Eng. C 37 (2014) 332–341.

[28] L. Gladczuk, A. Patel, C. Singh Paur, M. Sosnowski, Tantalum films for protective coatings of steel, Thin Solid Films 467 (2004) 150–157.

[29] T. Albrektsson, A. Wennerberg, Oral implant surfaces: Part 1 — review focusing on topographic and chemical properties of different surfaces and in vivo responses to them, Int. J. Prosthodont. 17 (2004) 536.

[30] Y. Leng, J. Chen, P. Yang, H. Sun, J. Wang, N. Huang, The biocompatibility of the tantalum and tantalum oxide films synthesized by pulse metal vacuum arc source deposition, Nucl. Inst. Methods Phys. Res. B 242 (2006) 30–32.

[31] W. Yang, Y. Liu, Q. Zhang, Y. Leng, H. Zhou, P. Yang, J. Chen, N. Huang, Biomedical response of tantalum oxide films deposited by DC reactive unbalanced magnetron sputtering, Surf. Coat. Technol. 201 (2007) 8062–8065.

[32] A. Zeller, A. Musyanovych, M. Kappl, A. Ethirajan, M. Dass, D. Markova, M. Klapper, K. Landfester, Nanostructured coatings by adhesion of phosphonated polystyrene particles onto titanium surface for implant material applications, ACS Appl. Mater. Interfaces 2 (2010) 2421–2428.

[33] M.G. Kutty, A. De, S.B. Bhaduri, A. Yaghoubi, Microwave-assisted fabrication of titanium implants with controlled surface topography for rapid bone healing, ACS Appl. Mater. Interfaces 6 (2014) 13587–13593.

[34] W.Z. Li, M. Evaristo, A. Cavaleiro, Influence of Al on the microstructure and mechanical properties of Cr–Zr–(Al–)N coatings with low and high Zr content, Surf. Coat. Technol. 206 (2012) 3764–3771.

[35] M. Hulander, J. Hong, M. Andersson, F. Gervén, M. Ohrlander, P. Tengvall, H. Elwing, Blood interactions with noble metals: coagulation and immune complement activation, ACS Appl. Mater. Interfaces 1 (2009) 1053–1062.

[36] C. Van Oss, R. Good, M. Chaudhury, The role of van der Waals forces and hydrogen bonds in "hydrophobic interactions" between biopolymers and low energy surfaces, J. Colloid Interface Sci. 111 (1986) 378–390.

[37] T. Kokubo, H. Takadama, How useful is SBF in predicting in vivo bone bioactivity? Biomaterials 27 (2006) 2907–2915.

[38] B. Wopenka, J.D. Pasteris, A mineralogical perspective on the apatite in bone, Mater. Sci. Eng. C 25 (2005) 131–143.

[39] S. Chandra, S. Uthanna, G.M. Rao, Effect of substrate temperature on the structural, optical and electrical properties of dc magnetron sputtered tantalum oxide films, Appl. Surf. Sci. 254 (2008) 1953–1960.

[40] D. Cristea, D. Constantin, A. Crisan, C. Abreu, J. Gomes, N. Barradas, E. Alves, C. Moura, F. Vaz, L. Cunha, Properties of tantalum oxynitride thin films produced by magnetron sputtering: the influence of processing parameters, Vacuum 98 (2013) 63–69.

[41] F. Vaz, P. Carvalho, L. Cunha, L. Rebouta, C. Moura, E. Alves, A.R. Ramos, A. Cavaleiro, P. Goudeau, J.P. Rivière, Property change in ZrNxOy thin films: effect of the oxygen fraction and bias voltage, Thin Solid Films 469–470 (2004) 11–17.

[42] M. Chandrasekhar, S.J. Chandra, S. Uthanna, Characterization of bias magnetron sputtered tantalum oxide films for capacitors, Indian J. Pure Appl. Phys. 47 (2009) 49–53.

[43] Y. Zhou, Z. Xie, H. Xiao, P. Hu, J. He, Effects of deposition parameters on tantalum films deposited by direct current magnetron sputtering, Vacuum 83 (2009) 286–291.

[44] Y. Zhou, Z. Xie, H. Xiao, P. Hu, J. He, Effects of deposition parameters on tantalum films deposited by direct current magnetron sputtering in Ar–O₂ mixture, Appl. Surf. Sci. 258 (2011) 1699–1703.

[45] R. Knepper, B. Stevens, S.P. Baker, Effect of oxygen on the thermomechanical behavior of tantalum thin films during the β–α phase transformation, J. Appl. Phys. 100 (2006) 123508–123511.

[46] N.M.G. Parreira, N.J.M. Carvalho, A. Cavaleiro, Synthesis, structural and mechanical characterization of sputtered tungsten oxide coatings, Thin Solid Films 510 (2006) 191–196.

[47] N.M.G. Parreira, N.J.M. Carvalho, F. Vaz, A. Cavaleiro, Mechanical evaluation of unbiased W–O–N coatings deposited by d.c. reactive magnetron sputtering, Surf. Coat. Technol. 200 (2006) 6511–6516.

[48] A.C. Fernandes, P. Carvalho, F. Vaz, S. Lanceros-Méndez, A. Machado, N. Parreira, J. Pierson, N. Martin, Property change in multifunctional TiCxOy thin films: effect of the O/Ti ratio, Thin Solid Films 515 (2006) 866–871.

[49] C. Oliveira, R.E. Galindo, C. Palacio, L. Vázquez, A. Espinosa, B. Almeida, M. Henriques, S. Carvalho, Influence of the surface morphology and microstructure on the biological properties of Ti–Si–C–N–O coatings, Thin Solid Films 518 (2010) 5694–5699.

[50] F. Guimarães, C. Oliveira, E. Sequeiros, M. Torres, M. Susano, M. Henriques, R. Oliveira, R. Escobar Galindo, S. Carvalho, N.M.G. Parreira, F. Vaz, A. Cavaleiro, Structural and Mechanical properties of Ti–Si–C–ON for biomedical applications, Surf. Coat. Technol. 202 (2008) 2403–2407.

[51] M. Ohring, Materials Science of Thin Films, Academic Press, 2001.

[52] O. Banakh, P.-A. Steinmann, L. Dumitrescu-Buforn, Optical and mechanical properties of tantalum oxynitride thin films deposited by reactive magnetron sputtering, Thin Solid Films 513 (2006) 136–141.

[53] N.M.G. Parreira, T. Polcar, A. Cavaleiro, Characterization of W–O coatings deposited by magnetron sputtering with reactive gas pulsing, Surf. Coat. Technol. 201 (2007) 5481–5486.

[54] J. Wei, T. Igarashi, N. Okumori, T. Igarashi, T. Maetani, B. Liu, M. Yoshinari, Influence of surface wettability on competitive protein adsorption and initial attachment of osteoblasts, Biomed. Mater. 4 (2009) 045002–045007.

[55] M.D. Mager, V. LaPointe, M.M. Stevens, Exploring and exploiting chemistry at the cell surface, Nat. Chem. 3 (2011) 582–589.

[56] K. Cai, M. Frant, J. Bossert, G. Hildebrand, K. Liefeith, K.D. Jandt, Surface functionalized titanium thin films: zeta-potential, protein adsorption and cell proliferation, Colloids Surf. B: Biointerfaces 50 (2006) 1–8.

[57] C.P. Sharma, W. Paul, Protein interaction with tantalum: changes with oxide layer and hydroxyapatite at the interface, J. Biomed. Mater. Res. 26 (1992) 1179–1184.

[58] G. Mendonça, D.B.S. Mendonça, F.J.L. Aragão, L.F. Cooper, Advancing dental implant surface technology — from micron- to nanotopography, Biomaterials 29 (2008) 3822–3835.

[59] L. Zhang, T.J. Webster, Nanotechnology and nanomaterials: promises for improved tissue regeneration, Nano Today 4 (2009) 66–80.

[60] G. Zhao, Z. Schwartz, M. Wieland, F. Rupp, J. Geis Gerstorfer, D. Cochran, B. Boyan, High surface energy enhances cell response to titanium substrate microstructure, J. Biomed. Mater. Res. Part A 74 (2005) 49–58.

[61] L. Bacakova, E. Filova, M. Parizek, T. Ruml, V. Svorcik, Modulation of cell adhesion, proliferation and differentiation on materials designed for body implants, Biotechnol. Adv. 29 (2011) 739–767.

[62] T. Kokubo, Formation of biologically active bone-like apatite on metals and polymers by a biomimetic process, Thermochim. Acta 280 (1996) 479–490.

[63] T. Kokubo, T. Matsushita, H. Takadama, T. Kizuki, Development of bioactive materials based on surface chemistry, J. Eur. Ceram. Soc. 29 (2009) 1267–1274.

[64] T. Kokubo, F. Miyaji, H.M. Kim, T. Nakamura, Spontaneous formation of bonelike apatite layer on chemically treated titanium metals, J. Am. Ceram. Soc. 79 (1996) 1127–1129.

[65] B. Feng, J. Weng, B. Yang, S. Qu, X. Zhang, Characterization of surface oxide films on titanium and adhesion of osteoblast, Biomaterials 24 (2003) 4663–4670.

[66] L. Calderin, M. Stott, A. Rubio, Electronic and crystallographic structure of apatites, Phys. Rev. B 67 (2003) 134106–134107.

[67] H. Li, W. Huang, Y. Zhang, M. Zhong, Biomimetic synthesis of enamel-like hydroxyapatite on self-assembled monolayers, Mater. Sci. Eng. C 27 (2007) 756–761.

[68] J. Shi, N.M. Alves, J.F. Mano, Thermally responsive biomineralization on biodegradable substrates, Adv. Funct. Mater. 17 (2007) 3312–3318.

[69] R. Murugan, S. Ramakrishna, Bioresorbable composite bone paste using polysaccharide based nano hydroxyapatite, Biomaterials 25 (2004) 3829–3835.

[70] E. Nejati, V. Firouzdor, M. Eslaminejad, F. Bagheri, Needle-like nano hydroxyapatite/poly (L-lactide acid) composite scaffold for bone tissue engineering application, Mater. Sci. Eng. C 29 (2009) 942–949.